Available online at http://scik.org
Commun. Math. Biol. Neurosci. 2025, 2025:29
https://doi.org/10.28919/cmbn/9138
ISSN: 2052-2541

# A FRACTIONAL MATHEMATICAL EXAMINATION ON BREAST CANCER PROGRESSION FOR THE HEALTHCARE SYSTEM OF JORDAN

IQBAL M. BATIHA[1,2,*], HAMZAH O. AL-KHAWALDEH[3], MANAL ALMUZINI[4,5], WASEEM G. ALSHANTI[1], NIDAL ANAKIRA[6,7], ALA AMOURAH[6,8]

[1]Department of Mathematics, Al Zaytoonah University of Jordan, Amman 11733, Jordan

[2]Nonlinear Dynamics Research Center (NDRC), Ajman University, Ajman, United Arab Emirates

[3]Department of Mathematics, Al Al-Bayt University, Mafraq, Jordan

[4]School of Mathematical Sciences, Universiti Sains Malaysia, Penang 11800, Malaysia

[5]Department of Mathematics and Statistics, American University of Sharjah, Sharjah 26666, United Arab Emirates

[6]Faculty of Education and Arts, Sohar University, Sohar 3111, Oman

[7]Applied Science Research Center, Applied Science Private University, Amman 11937, Jordan

[8]Jadara University Research Center, Jadara University, Jordan



**Abstract.** Breast cancer remains a significant public health challenge worldwide, with rising incidence rates in both developed and developing nations. This study presents a fractional mathematical model to examine the progression of breast cancer within the healthcare system of Jordan. The proposed model integrates fractional calculus to account for the non-linear dynamics and long-memory effects characteristic of biological systems. It employs a compartmental framework, categorizing women into six states: Susceptible, Preclinical, Clinical, Treatment, Remission, and Death. Transition rates between these states are derived from local epidemiological data to ensure relevance to Jordan's healthcare context. The model is analyzed for stability, disease-free equilibrium (DFEP), and endemic equilibrium (EEP), using fractional differential equations to explore the dynamics of breast cancer

*Corresponding author

E-mail address: i.batiha@zuj.edu.jo

Received January 18, 2025

progression. Numerical solutions are obtained using the Modified Fractional Euler Method (MFEM), showcasing the impact of various parameters on disease spread and treatment outcomes. Results emphasize the utility of fractional-order models in capturing the intricate interplay of biological and clinical factors influencing breast cancer dynamics. This study provides valuable insights for policymakers and healthcare professionals, facilitating the optimization of resource allocation and the development of targeted intervention strategies in Jordan.

**Keywords:** breast cancer progression; fractional calculus; compartmental model; stability analysis; healthcare system of Jordan.

**2020 AMS Subject Classification:** 03C65, 26A33.

## 1. INTRODUCTION

Globally, cancer is a major public health concern. Out of all the varieties of cancer that now exist, breast cancer is the most common and leading cause of cancer in women, and it continues to rise in both developed and developing countries [1, 2]. Breast cancer (BC) is the result of unchecked, malignant or benign breast cell proliferation. In contrast to the malignant cancer kinds, which include invasive lobular carcinoma, invasive ductal carcinoma, papillary carcinoma, and mucinous carcinoma, Benign cancer kinds are phyllodes, tubular adenoma tumor, adenosis, and fibroadenoma [3]. The most popular method for diagnosing breast cancer is the triple assessment test comprises of biopsy test, imaging, and clinical examination [4]. Because it can identify the type, sub-type, and stage of breast cancer, compared to medical imaging procedures such as mammography, MRI, ultrasound, and CT, the histopathological image (biopsy test) is the gold standard for diagnosing breast cancer [5]. Histopathological analysis is used to establish the existence or absence of disease as well as to grade the disease and determine how far along it is [6]. Breast cancer grading facilitates the assessment of the disease's aggressiveness, growth rate, and extent of dissemination. The three grades for breast tumors are 1. and 3. Grade 1 breast cancer cells are often slow-growing and resemble normal cells in homogeneity and size. Compared to normal cells, grade 2 cells are slightly larger, vary in shape, and grow more quickly. Similarly, Grade 3 cancer cells have a distinct appearance and typically proliferate more quickly than healthy cells [7, 8]. Because microscopic histopathological analysis is typically performed by eye inspection, its accuracy depends on how well the doctor performs. Because of this, multi-classifying breast cancer utilizing histological photos is a difficult

endeavor because it is subjective, the correctness of the results depends on the observer's experience and knowledge, and the process is time-consuming and laborious. Furthermore, because most underdeveloped nations lack skilled pathologists, every day, a pathologist is expected to examine a variety of biopsy samples from different cases. Owing to the limited pathologist's analysis of a wide range and volume of data, as well as the intricacy of the images, conclusions could be misinterpreted. Exaggerated or underinterpreted diagnosis are two possible types of misdiagnosis. Women who do not have cancer may be subjected harmful therapies and needless expenses as a result of misinterpretation. On the other side, if women fail to receive treatment at an early stage, the cancer may progress to more invasive stages due to incorrect or inadequate interpretation of the biopsy results. Furthermore, the enhanced multi-class classification of the disease type serves as the basis for choosing the optimal therapeutic approach for breast cancer. By employing therapeutic approaches, early control of tumor cell metastasis can be achieved with the accurate identification of breast cancer subclasses. However, the manual biopsy test approach may not be reliable for classifying breast cancer into multiple categories. The aforementioned issues can be resolved by using computer aided diagnostic (CAD) tools for breast cancer histology. Intelligent diagnostic algorithms can lessen the workload of pathologists while improving diagnosis accuracy and lowering the mistake rate in breast cancer type classification and grading [9, 10]. Designing appropriate histopathological image capture, intelligent feature extraction methodologies, and pre-processing is, however, a demanding task for computer-aided breast cancer detection [9]. Deep learning techniques can extract features from photos, automatically recognize visual patterns, and represent images in an abstract form that incorporates the most visible information needed to distinguish them from other similar images. Recent research has developed deep neural network (DNN) models for the diagnosis of breast cancer using histopathology images [11, 12]. A deep CNN-like patch level voting model and a merging model were used to categorize breast tissue biopsy images as normal, benign, malignant, or invasive cancer, with an accuracy of 87.5% [13]. Similarly, deep convolutional neural network (DCNN) and gradient boosted tree approach were used to categorize breast cancer into the fundamental four types, with an accuracy of $93.8 \pm 2.3\%$ and $87.2 \pm 2.6\%$, respectively [14]. Araujo et al. [15] used CNN to extract features and support vector machines to classify images

at different scales, including nuclei and tissue organization. The study reported an accuracy of 77.8% for all four classes and 83.3% for carcinoma (invasive and in situ) or non-carcinoma (benign and normal). The Inception-v3 convolutional neural network was fine-tuned for patch classification, and majority vote was employed for overall slide classification, resulting in an accuracy of 85% for all four classes and 93% for non-cancer (benign and normal) versus malignant (invasive carcinoma or in situ) [16].

Fractional calculus is becoming increasingly popular in medical systems, chemical, and biological [17]. It expands the usual, integer-order differential calculus to non-integer order [18, 19, 20]. Many scholars have already demonstrated that fractional order models are superior at describing this phenomenon, see [21, 22, 23, 24, 25, 26, 27]. Great achievements are provided in a variety of domains, including biosciences, bioengineering, economics, medicine, control, physics, neural networks, and signal processing [28, 29]. Many authors concur that fractional operators can help capture and explain the more relative repercussions of physical processes with increased non-linearity and complexity, as well as history-based properties and long-range memory [30]. In [31], the dynamics of a fractional partial differential equation model of the Zika virus are investigated. The authors use the Atangana-Baleanu fractional derivative to describe how the spread of humans and mosquitoes effects disease transmission.

Cancer is becoming more prevalent in our culture because it is one of the top causes of illness and death worldwide. Because of this, there are numerous treatment options available, including surgery, radiation therapy, chemotherapy, immunotherapy, hormone therapy, and anti-angiogenic therapy. For all of these treatments, it is important to weigh the pros, cons, and side effects of each treatment. As a result, a logical mathematical approach to cancer therapy is to examine a mathematical model of tumor temporal evolution that includes therapy action as a control mechanism, with the goal of reducing tumor volume while minimizing negative side effects on healthy cells. To select the best therapy, we formulate an optimal control problem that entails minimizing tumor volume over a certain time horizon while optimizing the patient's health-related quality of life [32].

## 2. BASIC FUNDAMENTALS

In this section, we will discuss certain definitions and properties of fractional calculus, which will pave the way for the important results later.

**Definition 2.1.** *Suppose $\sigma$ is a real, non-negative number. Then $J_a^\sigma$ defined on $L_1[a,b]$, where $L_1[a,b]$ is the set of all functions that whose absolute values are integrable on $[a,b]$ by* [33]*:*

$$J_a^\sigma \psi(s) = \frac{1}{\Gamma(\sigma)} \int_a^s (s-w)^{\sigma-1} \psi(w) dw,\ a \leq s \leq b, \tag{1}$$

*is referred to as the Riemann-Liouville fractional-order integral operator of order $\sigma$.*

In the following, we will mention several properties of the Riemann-Liouville fractional-order integral operator.

(1) Let $m,n \geq 0$ and $\psi \in L_1[a,b]$. Then we have: $J_a^m J_a^n \psi = J_a^{m+n} \psi$.

(2) For $m,n \geq 0$, we have: $J_a^m J_a^n \psi = J_a^n J_a^m \psi$.

(3) For $m,n \geq 0$, we have: $J_a^{m+n} \psi = J_a^{m+n-1} J_a^1 \psi$.

**Definition 2.2.** *Assume $\sigma \in \mathbb{R}$ and $r = \lceil \sigma \rceil$. The operator $D_a^\sigma$ is defined as:*

$$D_a^\sigma \psi = D^r J_a^{r-\sigma} \psi, \tag{2}$$

*is referred to as the Riemann-Liouville fractional-order differential operator of order $\sigma$.*

When $\gamma = 0$ in Equation (3), we obtain $D_a^0 = I$, also known as the Identity operator [34]. The next step is to present the main definition of the operator at hand.

**Definition 2.3.** *Assume $\sigma$ is a real, nonnegative number. The Riemann-Liouville fractional-order differential operator of a function $\psi$ of order $\sigma$ is defined as* [33] *for a positive integer $r$ with $r-1 < \sigma \leq r$:*

$$D_a^\sigma \psi(s) = \frac{1}{\Gamma(r-\sigma)} \frac{d^r}{ds^r} \int_a^s (s-w)^{r-\sigma-1} \psi(w) dw. \tag{3}$$

Without losing generality, assume $a = 0$ in Equation (3) to get:

$$D_0^\sigma \psi(s) = \frac{1}{\Gamma(r-\sigma)} \frac{d^r}{ds^r} \int_0^s (s-w)^{r-\sigma-1} f(w) dw. \tag{4}$$

The Riemann-Liouville fractional-order derivative of the function $\psi$ of order $\sigma$ is also defined by the following for $0 < \sigma \leq 1$:

$$D_0^{\sigma}\psi(s) = \frac{1}{\Gamma(1-\sigma)}\frac{d}{ds}\int_0^s (s-w)^{-\sigma}\psi(w)dw. \tag{5}$$

The Power Rule property can be deduced from Equation (5) and summarized as follows:

$$D_0^{\sigma}s^p = \frac{\Gamma(p+1)}{\Gamma(p-\sigma+1)}s^{p-\sigma}, \tag{6}$$

where $p \in \mathbb{R}$. Regarding this, it should be noted that a constant function $C$ has a fractional-order derivative that is not zero. Thus, [35]:

$$D_0^{\sigma}C = \frac{s^{-\sigma}}{\Gamma(1-\sigma)}C, \tag{7}$$

where $C$ is constant.

The Riemann-Liouville fractional-order derivative operator is discussed in detail in the following content. These properties can be used to illustrate how such an operator interacts with itself and the Riemann-Liouville integral operator.

(1) Consider $n \geq 0$. For every $\psi \in L_1[a,b]$, $D_a^n J_a^n \psi = \psi$ practically everywhere.

(2) Assume $\sigma_1, \sigma_2 \geq 0$ and $\phi \in L_1[a,b]$ such that $\psi = J_a^{\sigma_1+\sigma_2}\phi$. Then $D_a^{\sigma_1}D_a^{\sigma_2}\psi = D_a^{\sigma_1+\sigma_2}\psi$.

**Definition 2.4.** *Assume $r = \lceil \sigma \rceil$ and $\sigma \in \mathbb{R}$. The definition of the Caputo fractional derivative operator $D_a^{\sigma}$ is*

$$D_a^{\sigma}\psi = J_a^{r-\sigma}D^r\psi. \tag{8}$$

**Definition 2.5.** *Suppose $\sigma \in \mathbb{R}^+$ and $r = \lceil \sigma \rceil$ such that $r-1 < \sigma \leq r$. The Caputo fractional-order derivative operator of order $\sigma$ is given as* [33]

$$D_a^{\sigma}\psi(s) = \frac{1}{\Gamma(r-\sigma)}\int_a^s (s-\tau)^{r-\sigma-1}\psi^{(r)}(\tau)d\tau,\ s > a. \tag{9}$$

Equation (9) helps the following power rule property to be obtained:

$$D_*^{\sigma}s^p = \begin{cases} \frac{\Gamma(p+1)}{\Gamma(p-\sigma+1)}s^{p-\sigma} & ,\ r-1 < \sigma \leq r,\ p > r-1,\ p \in \mathbb{R} \\ 0 & ,\ r-1 < \sigma \leq r,\ p \leq r-1,\ p \in \mathbb{N}. \end{cases} \tag{10}$$

Following that, we'll go over some fundamental Caputo fractional-order derivative operator characteristics. These characteristics are connected to the linearity and non-commutativity of the operator under study.

(1) Let $r-1<\sigma\leq r$ such that $r\in\mathbb{N}$. Then

$$(D_a^{\sigma}(\lambda\psi(s)+\mu g(s)))=(\lambda D_a^{\sigma}\psi(s)+\mu D_a^{\sigma}g(s)),$$

where $\lambda$ and $\mu$ are two scalers.

(2) Let $r-1<\sigma\leq r$ such that $r,\beta\in\mathbb{N}$, and $\sigma\in\mathbb{R}$. Then

$$(D_a^{\sigma}D_a^{\beta}\psi(s))=(D_a^{\sigma+\beta}\psi(s))\neq(D_a^{\beta}D_a^{\sigma}\psi(s)).$$

**Theorem 2.6.** *Consider* ${}^{C}D_*^{i\sigma}\omega(x)\in C(0,T]$, *for* $i=0,1,2,\cdots,n+1$, *and* $0<\sigma\leq 1$. *The function* $\omega(x)$ *can be extended around* $x_0$ *in the following manner* [36]*:*

$$\omega(x)=\sum_{i=0}^{n}\frac{(x-x_0)^{i\sigma}}{\Gamma(i\sigma+1)}\left({}^{C}D_*^{i\sigma}\omega\right)(x_0)+\frac{(x-x_0)^{(n+1)\sigma}}{\Gamma((n+1)\sigma+1)}\left({}^{C}D_*^{(n+1)\sigma}\omega\right)(\zeta), \tag{11}$$

$\forall x\in(0,T]$, *where* $0<\zeta<x$.

## 3. Compartmental Model

To develop a proper mathematical model for the progression of breast cancer in Jordan's healthcare system, local data must be adapted to wide cancer modeling methodologies. To create a compartmental model, we assume the following compartments:

(1) Susceptible (S): Women who are at risk of developing breast cancer but do not currently have it.
(2) Preclinical (P):Women at the preclinical stage of breast cancer who have not received a diagnosis.
(3) Clinical (C): Women with a breast cancer diagnosis (clinical stage).
(4) Treatment (T): Women are receiving medical treatment.
(5) Remission (R): Women who have achieved remission after receiving effective treatment.
(6) Death (D): Women who have died of breast cancer.

To represent the transition between all the previous compartments, we established the following fractional differential equations:

(1) Susceptible to preclinical: The transition from susceptible to preclinical occurs at a rate that is proportional to the incidence rate ($\beta$), i.e.,

$$D_*^{\sigma} S(s) = -\beta S(s),$$

the incidence rate of breast cancer could be approximated by $\frac{60}{100000}$ women annually (0.0006).

(2) Preclinical to clinical: The rate of diagnosis of breast cancer drives the transition from preclinical to clinical ($\gamma$), i.e.,

$$D_*^{\sigma} P(s) = \beta S(s) - \gamma P(s),$$

the diagnosed rate ($\gamma$) shows the probability of transitioning from undiagnosed to diagnosed. This percentage can be approximated for Jordan's healthcare system by the value of 80% of cases detected at some point.

(3) Clinical to Treatment: The transition from clinical to therapy is driven by the rate at which diagnosed patients begin treatment ($\delta$), i.e.,

$$D_*^{\sigma} C(s) = \gamma P(s) - \delta C(s),$$

the treatment initiation rate $\delta$, representing the period from diagnosis to therapy, might be approximated by 70%.

(4) Treatment to Remission: The treatment success rate determines the transition from treatment to remission ($\alpha$), i.e.,

$$D_*^{\sigma} T(s) = \delta C(s) - \alpha T(s),$$

the treatment success rate $\alpha$, which indicates the remission rate, can be approximated as 65% of treated women achieving remission.

(5) Treatment to Death: The mortality rate determines the transition from treatment to death ($\mu$), i.e.,

$$D_*^{\sigma} T(s) = \delta C(s) - (\alpha + \mu) T(s),$$

for which the mortality rate from breast cancer in Jordan might be approximated by 10% of treated women die from the disease.

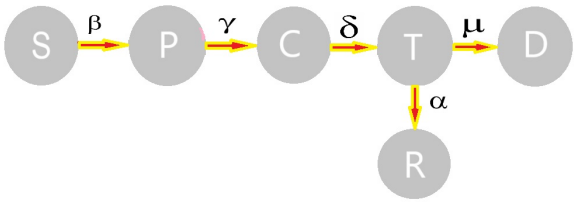


FIGURE 1. The compartmental model of the breast cancer for the healthcare system of Jordan.

(6) Remission to Recurrence: It should be mentioned that some women in remission may face cancer recurrence. This can be described using a recurrence rate ($\rho$), i.e.,

$$D_*^{\sigma} R(s) = \alpha T(s) - \rho R(s),$$

the recurrence rate $\rho$ can be approximated as 0.2, given that 20% of women in remission experience recurrence.

(7) Death: The compartment of death accumulates people who have died of breast cancer, i.e.,

$$D_*^{\sigma} D(s) = \mu T(s).$$

Based on the previous discussion, we can create the compartmental model for breast cancer progression for the Jordanian healthcare system, as shown in Figure 1.

In conclusion, the fractional-order model of breast cancer progression for a Jordanian healthcare system can be provided by

$$\begin{aligned}
D_*^{\sigma} S(s) &= (1-\theta) - \beta S(s), \\
D_*^{\sigma} P(s) &= \beta S(s) - \gamma P(s), \\
D_*^{\sigma} C(s) &= \gamma P(s) - \delta C(s), \\
D_*^{\sigma} T(s) &= \delta C(s) - (\alpha+\mu) T(s), \\
D_*^{\sigma} R(s) &= \alpha T(s) - \rho R(s), \\
D_*^{\sigma} D(s) &= \mu T(s),
\end{aligned} \tag{12}$$

where $\theta$ is the recruitment factor that represents a constant or rate at which new individuals enter the susceptible population (for example, through birth or immigration). To express the recruitment factor for breast cancer in Jordan, we could use the annual incidence rate per 100,000 women. Based on available data, a reasonable estimate for Jordan would be 50 cases per 100,000 women per year (i.e. 50/100,000).

It is critical to specify many key assumptions in regard to model (1). The assumptions are:

(1) The population size of women $N$ is about 5 million for Jordan. This value represents the initial susceptible population $S_0$, i.e. $S_0 = 5000000$.

(2) The estimated annual chance of having breast cancer among women is 0.1%. This value represents the initial clinical population $P_0$, i.e. $P_0 = 0.001$.

(3) The rest of the initial values are given in Table 1.

TABLE 1. caption

| Parameter | Value |
|---|---|
| $C_0$ | 1250 |
| $T_0$ | 2100 |
| $R_0$ | 12750 |
| $D_0$ | 2250 |

## 4. STABILITY ANALYSIS

In this section, we aim to examine the primary characteristics of model (12) in terms of numerous aspects including as basic reproduction number, the disease-free equilibrium point (DFEP), its stability, the endemic equilibrium point (EEP).

**4.1. Basic reproduction number ($R_0$).** The next-generation matrix approach (NGM) is used to evaluate the $R_0$, considering our infectious compartments are $P$, $C$, and $T$. Therefore, the infected subsystem can be formulated and written as follows:

$$Y = (P, C, T)^{\mathbf{T}},$$

$$\frac{dY}{ds} = M(Y) - N(Y).$$

Where we have:

$$M(Y) = \begin{pmatrix} \beta S(s) \\ 0 \\ 0 \end{pmatrix} \quad \text{and} \quad N(Y) = \begin{pmatrix} \gamma P(s) \\ -\gamma P(s) + \delta C(s) \\ -\delta C(s) + (\alpha + \mu) T(s) \end{pmatrix}$$

And find the Jacobian of both matrices around the DFEP yields:

$$\mathscr{M}(Y) = \begin{pmatrix} \beta S_0 & 0 & 0 \\ 0 & 0 & 0 \\ 0 & 0 & 0 \end{pmatrix} \quad \text{and} \quad \mathscr{N}(Y) = \begin{pmatrix} \gamma & 0 & 0 \\ -\gamma & \delta & 0 \\ 0 & -\delta & \alpha + \mu \end{pmatrix}$$

Thus, the $R_0$ is the spectral radius of $\mathscr{M}\mathscr{N}^{-1}$:

$$R_0 = \rho(MN^{-1}) = \rho\left( \begin{pmatrix} \beta S_0 & 0 & 0 \\ 0 & 0 & 0 \\ 0 & 0 & 0 \end{pmatrix} \cdot \begin{pmatrix} \frac{\alpha\delta+\delta\mu}{\alpha\gamma\delta+\gamma\delta\mu} & 0 & 0 \\ \frac{\alpha\gamma+\gamma\mu}{\alpha\gamma\delta+\gamma\delta\mu} & \frac{\alpha\gamma+\gamma\mu}{\alpha\gamma\delta+\gamma\delta\mu} & 0 \\ \frac{\gamma\delta}{\alpha\gamma\delta+\gamma\delta\mu} & \frac{\gamma\delta}{\alpha\gamma\delta+\gamma\delta\mu} & \frac{\gamma\delta}{\alpha\gamma\delta+\gamma\delta\mu} \end{pmatrix} \right)$$

$$= \frac{\beta S_0}{\gamma}.$$

Figures 2 and 3 illustrate the effects of key parameters, $\gamma$ (diagnosis rate) and $\beta$ (incidence rate), on the basic reproduction number $R_0$ within the proposed fractional-order breast cancer model. These visualizations demonstrate the sensitivity of $R_0$ to variations in these parameters, emphasizing their role in disease dynamics.

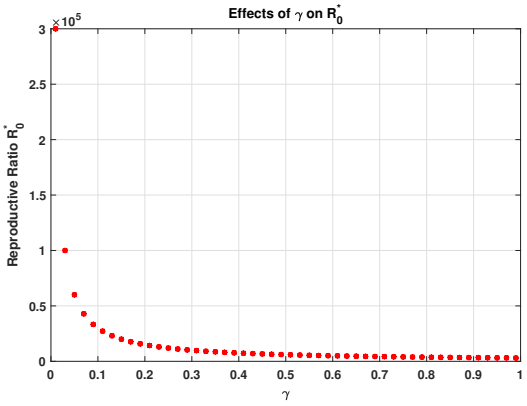


FIGURE 2. Code Effect of $\gamma$ parameter on $R_0$.

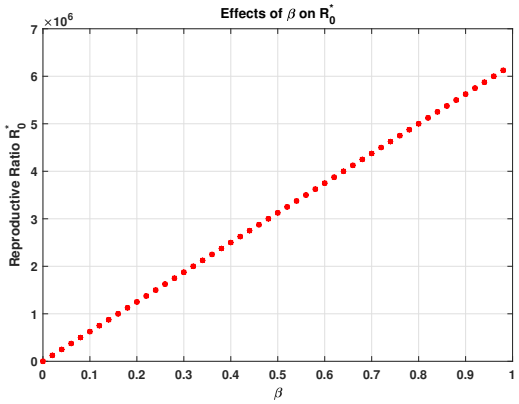


FIGURE 3. Code Effect of $\beta$ parameter on $R_0$.

In light of the above discussion, we observe that Figure 2 shows the inverse relationship between the diagnosis rate $\gamma$ and the basic reproduction number $R_0$. As $\gamma$ increases, $R_0$ decreases sharply, indicating that higher rates of diagnosis can significantly curb the disease's reproductive potential. This outcome aligns with the model's expectation that early and efficient detection reduces the susceptible population transitioning to advanced stages, thereby lowering overall disease prevalence. On the other hand, we note that Figure 3 demonstrates the direct proportionality between the incidence rate $\beta$ and $R_0$. As $\beta$ increases, $R_0$ rises exponentially, underscoring the impact of higher breast cancer incidence on the potential spread within the population. This behavior highlights the importance of public health measures aimed at reducing the risk factors associated with breast cancer development, as even slight increases in $\beta$ substantially elevate $R_0$.

**4.2. The disease-free equilibrium point (DFEP) and its stability.** The disease-free equilibrium point reflects the case where the human body has no cancer infection. Thus, the infection compartments should be equalized with zero value. Solving System in 12 for the healthy body yields the following DFEP:

$$DFEP = (S_0, P_0, C_0, T_0, R_0, D_0) = (S_0, 0, 0, 0, 0, 0)$$

Evaluating the Jacobian matrix for the system at the DFEP yields:

$$J(S_0,P_0,C_0,T_0,R_0,D_0) = \begin{pmatrix} -\beta & 0 & 0 & 0 & 0 & 0 \\ \beta & -\gamma & 0 & 0 & 0 & 0 \\ 0 & \gamma & -\delta & 0 & 0 & 0 \\ 0 & 0 & \delta & -\alpha-\mu & 0 & 0 \\ 0 & 0 & 0 & \alpha & -\rho & 0 \\ 0 & 0 & 0 & \mu & 0 & 0 \end{pmatrix}. \tag{13}$$

Then, we have the following Theorem for Local stability of the DFEP:

**Theorem 4.1.** *The disease-free equilibrium point DFEP of the proposed model 12 is considered to be a local asymptomatic stable if the following condition:*
$\lambda_i \leq 0$*, is satisfied for all eigenvalues of the matrix 13, where* $\lambda_i, i \in \{1,2,3,4,5,6\}$.

*Proof.* Under the condition that all applied parameters hold non-negative values, one can easily find the eigenvalues of the lower triangular Jacobian matrix to be evaluated as follows:
$\lambda_1 = -\beta < 0, \lambda_2 = -\gamma < 0, \lambda_3 = -\delta < 0, \lambda_4 = -(\alpha+\mu) < 0, \lambda_5 = -\rho < 0,$ and $\lambda_6 = 0$. Considering that $\lambda_6$ reflects the death compartment and ensures that there is no inflow or outflow for this compartment and, consequently, does not affect the stability. □

**4.3. The endemic equilibrium point (EEP).** The endemic or steady state equilibrium point exists when the disease persists within the community, assuming that infectious compartments hold non-zero values. Solving our system 12 where we have $P \neq 0$, $C \neq 0$, and $T \neq 0$, yields the following EEP:

$$(S^*,P^*,C^*,T^*,R^*,D^*) = \left(\frac{1-\theta}{\beta}, \frac{1-\theta}{\gamma}, \frac{1-\theta}{\delta}, \frac{1-\theta}{\alpha+\mu}, \frac{\alpha(1-\theta)}{\rho(\alpha+\mu)}, \frac{\mu(1-\theta)}{\alpha+\mu}\right)$$

Global stability of the EEP can be investigated by applying Ulam-Hyers approach [37] of the fractional model system defined in 12.

**Theorem 4.2.** *The System 12 is globally stable in the sense of Ulam-Hyers if and only if there* $\exists$ *a constant* $C > 0$ *such that*

$$\|\tilde{X}(s) - X(s)\| \leq C \cdot \max_{i=1,\ldots,6} \sup |\varepsilon_i(s)|.$$

*Where $\tilde{X}(s)$ is the perturbed solution of the system and $X(s)$ is the unperturbed solution.*

*Proof.* Let assume our perturbed system to be defined as:

$$\begin{aligned}
D_*^{\sigma}\tilde{S}(s) &= (1-\theta) - \beta\tilde{S}(s) + \varepsilon_1(s),\\
D_*^{\sigma}\tilde{P}(s) &= \beta\tilde{S}(s) - \gamma\tilde{P}(s) + \varepsilon_2(s),\\
D_*^{\sigma}\tilde{C}(s) &= \gamma\tilde{P}(s) - \delta\tilde{C}(s) + \varepsilon_3(s),\\
D_*^{\sigma}\tilde{T}(s) &= \delta\tilde{C}(s) - (\alpha+\mu)\tilde{T}(s) + \varepsilon_4(s),\\
D_*^{\sigma}\tilde{R}(s) &= \alpha\tilde{T}(s) - \rho\tilde{R}(s) + \varepsilon_5(s),\\
D_*^{\sigma}\tilde{D}(s) &= \mu\tilde{T}(s) + \varepsilon_6(s),
\end{aligned} \tag{14}$$

assuming that $\varepsilon_i(s)$ where $i \in 1,2,3,4,5,6$ are small perturbations.

Let $\tilde{X}(s)$ and $X(s)$ represent the approximate and exact solutions of the perturbed and unperturbed solutions of the system. Then we have:

$$\tilde{X}(s) = (\tilde{S}(s), \tilde{P}(s), \tilde{C}(s), \tilde{T}(s), \tilde{R}(s), \tilde{S}(s))$$

$$X(s) = (S^*(s), P^*(s), C^*(s), T^*(s), R^*(s), D^*(s)).$$

Our aim in the following analysis is to show that the absolute error between the approximate and exact solution ($e(s) = \tilde{X}(s)$-X(s)) remains bounded and small over time. Then the error functions will be founded as:

$$\begin{aligned}
e_S(s) &= \tilde{S}(s) - S^*(s),\\
e_P(s) &= \tilde{P}(s) - P^*(s),\\
e_C(s) &= \tilde{C}(s) - C^*(s),\\
e_T(s) &= \tilde{T}(s) - T^*(s),\\
e_R(s) &= \tilde{R}(s) - R^*(s),\\
e_D(s) &= \tilde{D}(s) - D^*(s).
\end{aligned} \tag{15}$$

Then, the system controlling the error terms will be as follows:

$$\begin{aligned}
D_*^{\sigma}e_S(s) &= -\beta e_S(s) + \varepsilon_1(s),\\
D_*^{\sigma}e_P(s) &= \beta e_S(s) - \gamma e_P(s) + \varepsilon_2(s),
\end{aligned}$$

$$
\begin{aligned}
D_*^{\sigma} e_C(s) &= \gamma e_P(s) - \delta e_C(s) + \varepsilon_3(s),\\
D_*^{\sigma} e_T(s) &= \delta e_C(s) - (\alpha+\mu) e_T(s) + \varepsilon_4(s),\\
D_*^{\sigma} e_R(s) &= \alpha e_T(s) - \rho e_R(s) + \varepsilon_5(s),\\
D_*^{\sigma} e_D(s) &= \mu e_T(s) + \varepsilon_6(s).
\end{aligned} \tag{16}
$$

Solving the last Equation 16, by the Mittag-Leffler function for the six compartments, one can easily find the constant C that depends on the parameters, fractional order, maximum value of the perturbation ($\varepsilon_i(s)$) error terms initial conditions. The general error of the system is represented by:

$$e(s) = (e_S(s), e_P(s), e_C(s), e_T(s), e_R(s), e_D(s)).$$

Hence, the error is bounded and can be represented by the following inequality:

$$\|e(s)\| \leq C \cdot \max_{i=1,\ldots,6} \sup |\varepsilon_i(s)|.$$

□

## 5. NUMERICAL FINDINGS

In the next content, we plan to utilize the numerical method MFEM to get the approximate solutions of the fractional-order Mpox system (12). In fact, these method represent fractional version of the conventional Euler method. A person can read the paper [38] in order to get clear idea about such method. In this context, Theorem 2.6 can lay the foundation to recall the MFEM, which are considered for the following fractional problem:

$$ {}^{C}D_*^{\sigma} \omega(x) = \Psi(s, \omega(s)),\ \omega(0) = \omega_0,\ s > 0,\ 0 < \sigma \leq 1. \tag{17}$$

To solve problem (17), we use $[0,a]$ as the interval to acquire the necessary numerical solution. In general, we are unable to identify $\omega(s)$, which reflects the analytical solution to the problem at hand. Alternatively, we may create a set of points $(s_i, \omega(s_i))$ and use them to construct an approximate solution [39, 40]. To simplify, we split $[0,a]$ into $k$ sub-intervals, $[s_i, s_{i+1}]$. with $h = \frac{a}{k}$ via $s_i = ih$, where $i = 0,1,2,\cdots,k$. We assume that $\omega(s)$, ${}^{C}D_*^{\sigma}\omega(s)$, and ${}^{C}D_*^{2\sigma}\omega(s)$ are continuous on $(0,a]$. Using Theorem 2.6, we may extend $\omega(s)$ around $s = s_i$ as follows

$$\omega(s) = \omega(s_i) + \frac{(s-s_i)^{\sigma}}{\Gamma(\sigma+1)} {}^{C}D_{*}^{\sigma}\omega(s_i) + \frac{(s-s_i)^{2\sigma}}{\Gamma(2\sigma+1)} {}^{C}D_{*}^{2\sigma}\omega(\zeta), \tag{18}$$

for some $\zeta \in (s_i,\ s_{i+1})$. Thus, if we substitute $s_{i+1}$ instead of $s$ in (18), we obtain

$$\omega(s_{i+1}) = \omega(s_i) + \frac{h^{\sigma}}{\Gamma(\sigma+1)} {}^{C}D_{*}^{\sigma}\omega(s_i) + \frac{(s_{i+1}-s_i)^{2\sigma}}{\Gamma(2\sigma+1)} {}^{C}D_{*}^{2\sigma}\omega(\zeta), \tag{19}$$

for some $\zeta \in (s_i,\ s_{i+1})$. Now, if one chooses $h = s_{i+1} - s_i$ too small, then the last term of (19) can be eliminated to obtain

$$\omega(s_{i+1}) = \omega(s_i) + \frac{h^{\sigma}}{\Gamma(\sigma+1)} {}^{C}D_{*}^{\sigma}\omega(s_i). \tag{20}$$

Actually, Equation (20) represents the primary formula of the FEM. In the same regard, if one substitutes

$${}^{C}D_{*}^{\sigma}\omega(s_{i+1}) = \Psi\left(s_i + \frac{h^{\sigma}}{\Gamma(\sigma+1)}, \omega(s_i) + \frac{h^{\sigma}}{\Gamma(\sigma+1)}\Psi(s_i, \omega(s_i))\right)$$

instead of (20), the result of $\omega(s_{i+1})$ will be consequently yielded. In other words, we obtain

$$\omega(s_{i+1}) = \omega(s_i) + \frac{h^{\sigma}}{\Gamma(\sigma+1)} \times \Psi\left(s_i + \frac{h^{\sigma}}{\Gamma(\sigma+1)}, \omega(s_i) + \frac{h^{\sigma}}{\Gamma(\sigma+1)}\Psi(s_i, \omega(s_i))\right), \tag{21}$$

for $i = 0, 1, 2, \cdots, k-1$. Equation (21) is the main formula of the MFEM, which will be compared with the FEM's formula. In the following, we attempt to implement only the MFEM on the fractional-order Mpox system (12), as the FEM and MFEM are identical. To do this, we must evaluate such a system as

$$\begin{aligned}
D_{*}^{\sigma}S(s) &= \Psi_1(s, S(s), P(s), C(s), T(s), R(s), D(s)) \\
D_{*}^{\sigma}P(s) &= \Psi_2(s, S(s), P(s), C(s), T(s), R(s), D(s)) \\
D_{*}^{\sigma}C(s) &= \Psi_3(s, S(s), P(s), C(s), T(s), R(s), D(s)) \\
D_{*}^{\sigma}T(s) &= \Psi_4(s, S(s), P(s), C(s), T(s), R(s), D(s)) \\
D_{*}^{\sigma}R(s) &= \Psi_5(s, S(s), P(s), C(s), T(s), R(s), D(s)) \\
D_{*}^{\sigma}D(s) &= \Psi_6(s, S(s), P(s), C(s), T(s), R(s), D(s)),
\end{aligned} \tag{22}$$

where

$$
\begin{aligned}
&\Psi_1(s,S(s),P(s),C(s),T(s),R(s),D(s)) = (1-\theta)-\beta S(s)\\
&\Psi_2(s,S(s),P(s),C(s),T(s),R(s),D(s)) = \beta S(s)-\gamma P(s)\\
&\Psi_3(s,S(s),P(s),C(s),T(s),R(s),D(s)) = \gamma P(s)-\delta C(s)\\
&\Psi_4(s,S(s),P(s),C(s),T(s),R(s),D(s)) = \delta C(s)-(\alpha+\mu)T(s)\\
&\Psi_5(s,S(s),P(s),C(s),T(s),R(s),D(s)) = \alpha T(s)-\rho R(s)\\
&\Psi_6(s,S(s),P(s),C(s),T(s),R(s),D(s)) = \mu T(s).
\end{aligned}
\tag{23}
$$

More precisely, with the view to obtaining $(s_k, S(s_k))$ in relation to compartment $S$, it should be assumed that $S(s)$, ${}^{C}D_{*}^{\sigma}S(s)$ and ${}^{C}D_{*}^{2\sigma}S(s)$ are continuous on $(0,T]$. From this point of view, if it can be supposed that

$$\Psi_1(s,S(s),P(s),C(s),T(s),R(s),D(s)) = -\beta S(s),$$

so that

$$D_{*}^{\sigma}S(s) = \Psi_1(s,S(s),P(s),C(s),T(s),R(s),D(s)),$$

then, with the use of (21), one might obtain

$$S(s_{i+1}) = S(s_i) + \frac{h^{\sigma}}{\Gamma(\sigma+1)} \times \Psi_1\left(s_i + \frac{h^{\sigma}}{\Gamma(\sigma+1)}, S(s_i) + \frac{h^{\sigma}}{\Gamma(\sigma+1)}\Psi_1(s_i, S(s_i))\right), \tag{24}$$

for $i = 0,1,2,...,k-1$.

Likewise, for the other classes the same approach might be used to arrive at an approximation of the solutions classes. In the long run, we can infer the following approximations of model (12):

$$
\begin{aligned}
S(s_{i+1}) &= S(s_i) + \frac{h^{\sigma}}{\Gamma(\sigma+1)} \times \Psi_1\left(s_i + \frac{h^{\sigma}}{\Gamma(\sigma+1)}, S(s_i) + \frac{h^{\sigma}}{\Gamma(\sigma+1)}\Psi_1(s_i, S(s_i))\right),\\
P(s_{i+1}) &= P(s_i) + \frac{h^{\sigma}}{\Gamma(\sigma+1)} \times \Psi_2\left(s_i + \frac{h^{\sigma}}{\Gamma(\sigma+1)}, P(s_i) + \frac{h^{\sigma}}{\Gamma(\sigma+1)}\Psi_2(s_i, P(s_i))\right),\\
C(s_{i+1}) &= C(s_i) + \frac{h^{\sigma}}{\Gamma(\sigma+1)} \times \Psi_3\left(s_i + \frac{h^{\sigma}}{\Gamma(\sigma+1)}, C(s_i) + \frac{h^{\sigma}}{\Gamma(\sigma+1)}\Psi_3(s_i, C(s_i))\right),\\
T(s_{i+1}) &= T(s_i) + \frac{h^{\sigma}}{\Gamma(\sigma+1)} \times \Psi_4\left(s_i + \frac{h^{\sigma}}{\Gamma(\sigma+1)}, T(s_i) + \frac{h^{\sigma}}{\Gamma(\sigma+1)}\Psi_4(s_i, T(s_i))\right),
\end{aligned}
\tag{25}
$$

$$R(s_{i+1}) = R(s_i) + \frac{h^\sigma}{\Gamma(\sigma+1)} \times \Psi_5 \left( s_i + \frac{h^\sigma}{\Gamma(\sigma+1)}, R(s_i) + \frac{h^\sigma}{\Gamma(\sigma+1)} \Psi_5(s_i, R(s_i)) \right),$$

$$D(s_{i+1}) = D(s_i) + \frac{h^\sigma}{\Gamma(\sigma+1)} \times \Psi_6 \left( s_i + \frac{h^\sigma}{\Gamma(\sigma+1)}, D(s_i) + \frac{h^\sigma}{\Gamma(\sigma+1)} \Psi_6(s_i, D(s_i)) \right),$$

where $\Psi_1, \Psi_2, \Psi_3, \Psi_4, \Psi_5, \Psi_6$ are already outlined in (23), $i = 0, 1, 2, ..., k-1$.

The following content presents numerical findings that show the dynamics of the fractional-order Mpox system (12). In this connection, we consider Table 2, which draws very close data to certain accessible data gathered out of the Indian community, on the basis of reference [41, 42].

TABLE 2. Parameters of system

| Parameter | Value |
|---|---|
| S(0) | 5000000 |
| P(0) | 0.001 |
| C(0) | 1250 |
| T(0) | 2100 |
| R(0) | 12750 |
| D(0) | 2250 |
| $\beta$ | 0.0006 |
| $\gamma$ | 0.8 |
| $\delta$ | 0.7 |
| $\alpha$ | 0.65 |
| $\mu$ | 0.1 |
| $\rho$ | 0.2 |

Figures 4, 5, 6, 7, 8, and 9 depict the temporal evolution of various compartments in the fractional-order breast cancer model for different fractional orders $\sigma = 0.2, 0.4, 0.6, 0.8, 1$. These figures illustrate the dynamic changes in population sizes for the compartments: Susceptible, Preclinical, Clinical, Treatment, Remission, and Death over time.

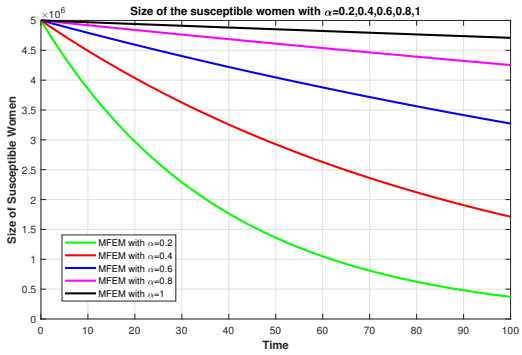


FIGURE 4. Size of the susceptible women with $\sigma = 0.2, 0.4, 0.6, 0.8, 1$

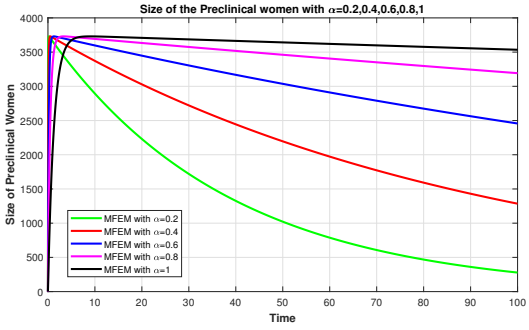


FIGURE 5. Size of the Preclinical women with $\sigma = 0.2, 0.4, 0.6, 0.8, 1$

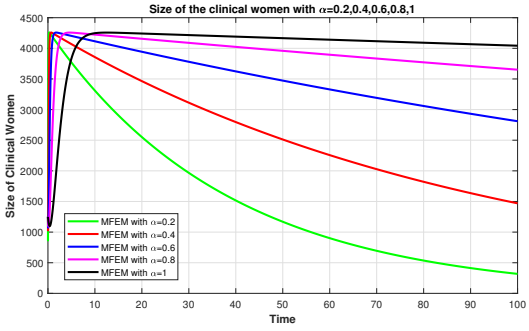


FIGURE 6. Size of the clinical women with $\sigma = 0.2, 0.4, 0.6, 0.8, 1$

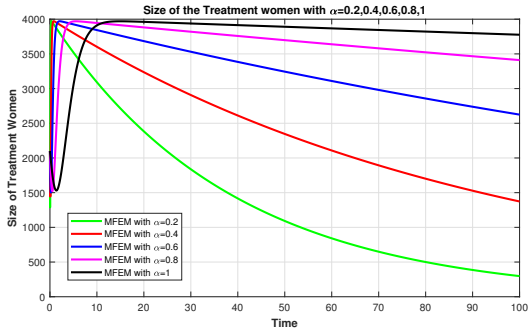


FIGURE 7. Size of the Treatment women with $\sigma = 0.2, 0.4, 0.6, 0.8, 1$

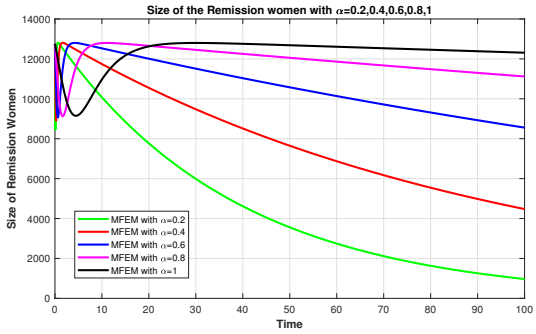


FIGURE 8. Size of the Remission women with $\sigma = 0.2, 0.4, 0.6, 0.8, 1$

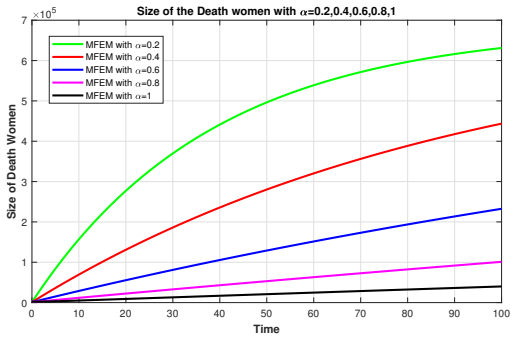


FIGURE 9. Size of the Death women with $\sigma = 0.2, 0.4, 0.6, 0.8, 1$

Figure 4 shows a gradual decline in the susceptible population over time, with slower decreases observed at lower fractional orders $\sigma = 0.2, 0.4$. Higher fractional orders $\sigma = 0.8, 1$ result in a steeper decline, reflecting more rapid transitions out of the susceptible compartment due to the disease's progression. In Figure 5, we observe that the preclinical compartment peaks

initially before declining, demonstrating the transition from undiagnosed cases to diagnosis and subsequent treatment. Higher fractional orders $\sigma = 0.8, 1$ result in faster transitions, shortening the time preclinical cases remain undetected.In Figure 6, we observe that the clinical compartment increases and then stabilizes or decreases depending on the fractional order. Faster progression (higher $\sigma$) leads to quicker movement to treatment or death, reflecting the efficacy of diagnosis and therapy. In Figure 7, the treatment compartment experiences a steady increase and then stabilizes, with the rate of stabilization varying by $\sigma$. Higher fractional orders signify more women being treated earlier, showcasing the model's ability to simulate improved intervention timelines. In Figure 8, we note that the remission compartment grows over time, with higher $\sigma$ leading to earlier and larger accumulations of women achieving remission. This trend underscores the model's potential for evaluating treatment efficacy and recovery rates. Finally, in Figure 9, we observe that the death compartment shows a gradual increase over time, with lower $\sigma$ leading to slower growth. This trend indicates that fractional dynamics can delay or accelerate mortality, reflecting the interplay between diagnosis, treatment success, and disease severity.

Figures 10, 11, 12, and 13 present the temporal dynamics of the model's compartments grouped as "active states" (Preclinical, Clinical, Treatment, and Remission) and "extreme states" (Susceptible and Death). They compare these dynamics under fractional orders $\sigma = 0.5$ and $\sigma = 1$ to highlight the effects of fractional calculus on population transitions.

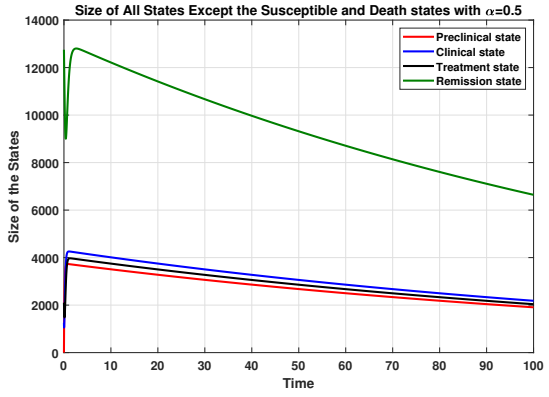


FIGURE 10. All states except $S$ and $D$ when $\sigma = 0.5$

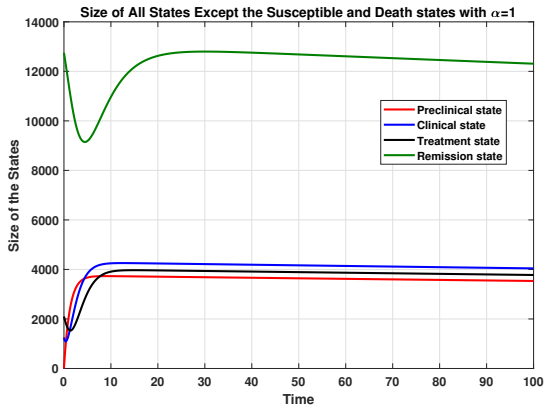


FIGURE 11. All states except $S$ and $D$ when $\sigma = 1$

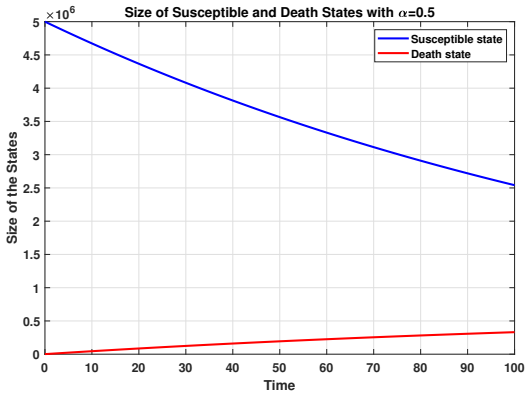


FIGURE 12. Size of Susceptible and Death States with $\sigma = 0.5$

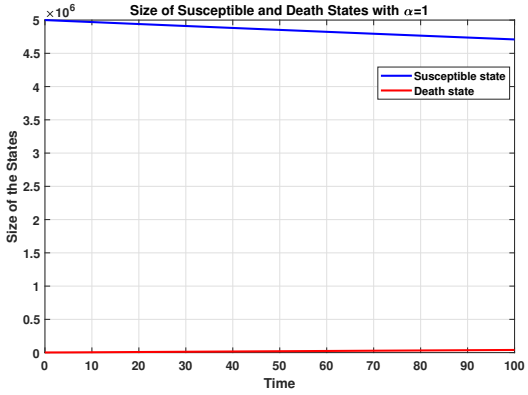


FIGURE 13. Size of Susceptible and Death States with $\sigma = 1$

In Figure 10, we observe that the Preclinical state peaks first, followed by peaks in Clinical and Treatment states, with the Remission state showing a continuous rise. This indicates a slower disease progression and prolonged transitions between compartments due to the fractional dynamics at $\sigma = 0.5$. In Figure 11, for $\sigma = 1$, the transitions between states are quicker, leading to earlier stabilization of the active compartments. This reflects a scenario with more deterministic dynamics where intervention measures are implemented more efficiently. In Figure 12, the susceptible population decreases gradually, while the death state grows steadily but remains subdued, reflecting slower disease spread and mortality under fractional dynamics at $\sigma = 0.5$. In Figure 13, the susceptible population shows a steeper decline, while the death compartment grows faster than in Figure 12. This highlights the impact of integer-order dynamics $\sigma = 1$ in accelerating disease progression and mortality.

## 6. Conclusion

This study presents a fractional-order mathematical model for breast cancer progression within the healthcare system of Jordan, incorporating compartments for different disease stages. The model leverages fractional calculus to capture non-linear dynamics and long-memory effects, providing a realistic representation of disease behavior. Stability analysis confirms the model's capability to predict disease-free and endemic equilibrium points. Numerical findings demonstrate the impact of key parameters, including fractional order, on population dynamics across compartments. The results highlight the potential of early diagnosis and effective treatment to reduce disease burden. The flexibility of fractional-order models makes them valuable for understanding complex biological systems and optimizing healthcare strategies. This work provides insights for policymakers to enhance resource allocation and intervention planning for breast cancer management.

### Acknowledgements

We acknowledge Al-Zaytoonah University of Jordan for funding this project under grant number (18/07/2023-2024).

### Conflict of Interests

The authors declare that there is no conflict of interests.

## REFERENCES

[1] N. Li, Y. Deng, L. Zhou, et al. Global Burden of Breast Cancer and Attributable Risk Factors in 195 Countries and Territories, from 1990 to 2017: Results from the Global Burden of Disease Study 2017, J. Hematol. Oncol. 12 (2019), 140. https://doi.org/10.1186/s13045-019-0828-0.

[2] Global Burden of Disease Cancer Collaboration, Global, Regional, and National Cancer Incidence, Mortality, Years of Life Lost, Years Lived With Disability, and Disability-Adjusted Life-Years for 29 Cancer Groups, 1990 to 2016: A Systematic Analysis for the Global Burden of Disease Study, JAMA Oncol. 4 (2018), 1553. https://doi.org/10.1001/jamaoncol.2018.2706.

[3] H. Tsuda, General Rule Committee of the Japanese Breast Cancer Society, Histological Classification of Breast Tumors in the General Rules for Clinical and Pathological Recording of Breast Cancer (18th Edition), Breast Cancer 27 (2020), 309–321. https://doi.org/10.1007/s12282-020-01074-3.

[4] Y.J. Zhang, L. Wei, J. Li, et al. Status Quo and Development Trend of Breast Biopsy Technology, Gland Surg. 2 (2013), 15–24. https://doi.org/10.3978/j.issn.2227-684X.2013.02.01.

[5] R. Rubin, D.S. Strayer, E. Rubin (Eds.), Rubin's Pathology: Clinicopathologic Foundations of Medicine, Lippincott Williams & Wilkins, (2008).

[6] M.N. Gurcan, L.E. Boucheron, A. Can, et al. Histopathological Image Analysis: A Review, IEEE Rev. Biomed. Eng. 2 (2009), 147–171. https://doi.org/10.1109/RBME.2009.2034865.

[7] K. Kuppusamy, A. Rajan, A. Warrier, et al. Cytological Grading of Breast Tumors—The Human and Canine Perspective, Front. Vet.Sci. 6 (2019), 283. https://doi.org/10.3389/fvets.2019.00283.

[8] C.W. Elston, I.O. Ellis, Classification of Malignant Breast Disease, in: Systemic Pathology, Churchill Livingstone, Edinburgh, pp. 239–247, 1998.

[9] L. Hadjiiski, B. Sahiner, H.-P. Chan, Advances in Computer-Aided Diagnosis for Breast Cancer, Curr. Opin. Obstet. Gynecol. 18 (2006), 64–70. https://doi.org/10.1097/01.gco.0000192965.29449.da.

[10] C. Kaushal, S. Bhat, D. Koundal, A. Singla, Recent Trends in Computer Assisted Diagnosis (CAD) System for Breast Cancer Diagnosis Using Histopathological Images, IRBM 40 (2019), 211–227. https://doi.org/10.1016/j.irbm.2019.06.001.

[11] J. Xie, R. Liu, J. Luttrell, C. Zhang, Deep Learning Based Analysis of Histopathological Images of Breast Cancer, Front. Genet. 10 (2019), 80. https://doi.org/10.3389/fgene.2019.00080.

[12] C. Zhu, F. Song, Y. Wang, H. Dong, Y. Guo, J. Liu, Breast Cancer Histopathology Image Classification through Assembling Multiple Compact CNNs, BMC Med. Inform. Decis. Mak. 19 (2019), 198. https://doi.org/10.1186/s12911-019-0913-x.

[13] Y. Guo, H. Dong, F. Song, C. Zhu, J. Liu, Breast Cancer Histology Image Classification Based on Deep Neural Networks, in: A. Campilho, F. Karray, B. Ter Haar Romeny (Eds.), Image Analysis and Recognition, Springer, Cham, 2018: pp. 827–836. https://doi.org/10.1007/978-3-319-93000-8_94.

[14] A. Rakhlin, A. Shvets, V. Iglovikov, A.A. Kalinin, Deep Convolutional Neural Networks for Breast Cancer Histology Image Analysis, in: A. Campilho, F. Karray, B. Ter Haar Romeny (Eds.), Image Analysis and Recognition, Springer, Cham, 2018: pp. 737–744. https://doi.org/10.1007/978-3-319-93000-8_83.

[15] T. Araújo, G. Aresta, E. Castro, et al. Classification of Breast Cancer Histology Images Using Convolutional Neural Networks, PLOS ONE 12 (2017), e0177544. https://doi.org/10.1371/journal.pone.0177544.

[16] A. Golatkar, D. Anand, A. Sethi, Classification of Breast Cancer Histology Using Deep Learning, in: A. Campilho, F. Karray, B. Ter Haar Romeny (Eds.), Image Analysis and Recognition, Springer, Cham, 2018: pp. 837–844. https://doi.org/10.1007/978-3-319-93000-8_95.

[17] E.-H. Dulf, F.-V. Dulf, C.-I. Muresan, Fractional Model of the Cryogenic $(^{13}C)$ Isotope Separation Column, Chem. Eng. Commun. 202 (2015), 1600–1606. https://doi.org/10.1080/00986445.2014.968709.

[18] N.R. Anakira, A. Almalki, D. Katatbeh, et al. An Algorithm for Solving Linear and Non-Linear Volterra Integro-Differential Equations, Int. J. Adv. Soft Comput. Appl. 15 (2023), 69–83.

[19] G. Farraj, B. Maayah, R. Khalil, W. Beghami, An Algorithm for Solving Fractional Differential Equations Using Conformable Optimized Decomposition Method, Int. J. Adv. Soft Comput. Appl. 15 (2023), 187–196.

[20] M. Berir, Analysis of the Effect of White Noise on the Halvorsen System of Variable-Order Fractional Derivatives Using a Novel Numerical Method, Int. J. Adv. Soft Comput. Appl. 16 (2024), 294–306.

[21] I.M. Batiha, S. Alshorm, M. Almuzini, Solving Fractional-Order Monkeypox Model by New Numircal Methods, in: A. Burqan, R. Saadeh, A. Qazza, et al. (Eds.), Mathematical Analysis and Numerical Methods, Springer, Singapore, 2024: pp. 551–561. https://doi.org/10.1007/978-981-97-4876-1_38.

[22] I. Jebril, S. Alshorm, I.M. Batiha, Numerical Solution for Fractional-Order Glioblastoma Multiforme Model, in: A. Burqan, R. Saadeh, A. Qazza, et al. (Eds.), Mathematical Analysis and Numerical Methods, Springer, Singapore, 2024: pp. 599–607. https://doi.org/10.1007/978-981-97-4876-1_42.

[23] I.M. Batiha, A.A. Abubaker, I.H. Jebril, et al. A Mathematical Study on a Fractional-Order SEIR Mpox Model: Analysis and Vaccination Influence, Algorithms 16 (2023), 418. https://doi.org/10.3390/a16090418.

[24] M. Abu Hammad, I.H. Jebril, S. Alshorm, I.M. Batiha, N. Abu Hammad, Numerical Solution for Fractional-Order Mathematical Model of Immune-Chemotherapeutic Treatment for Breast Cancer Using Modified Fractional Formula, Int. J. Anal. Appl. 21 (2023), 89. https://doi.org/10.28924/2291-8639-21-2023-89.

[25] I.M. Batiha, R. El-Khazali, O.Y. Ababneh, A. Ouannas, R.M. Batyha, S. Momani, Optimal Design of $PI^{\rho}D^{\mu}$-Controller for Artificial Ventilation Systems for COVID-19 Patients, AIMS Math. 8 (2023), 657–675. https://doi.org/10.3934/math.2023031.

[26] I.M. Batiha, A. Obeidat, S. Alshorm, et al. A Numerical Confirmation of a Fractional-Order COVID-19 Model's Efficiency, Symmetry 14 (2022), 2583. https://doi.org/10.3390/sym14122583.

[27] A. Dababneh, N. Djenina, A. Ouannas, et al. A New Incommensurate Fractional-Order Discrete COVID-19 Model with Vaccinated Individuals Compartment, Fractal Fract. 6 (2022), 456. https://doi.org/10.3390/fractalfract6080456.

[28] E.-H. Dulf, Simplified Fractional Order Controller Design Algorithm, Mathematics 7 (2019), 1166. https://doi.org/10.3390/math7121166.

[29] E.H. Dulf, C.I. Pop, F.V. Dulf, Fractional Calculus in $^{13}C$ Separation Column Control, Signal, Image and Video Processing 6 (2012), 479–485. https://doi.org/10.1007/s11760-012-0335-z.

[30] P. Veeresha, H.M. Baskonus, W. Gao, Strong Interacting Internal Waves in Rotating Ocean: Novel Fractional Approach, Axioms 10 (2021), 123. https://doi.org/10.3390/axioms10020123.

[31] P. Veeresha, L. Akinyemi, K. Oluwasegun, et al. Numerical Surfaces of Fractional Zika Virus Model with Diffusion Effect of Mosquito-borne and Sexually Transmitted Disease, Math. Methods Appl. Sci. 45 (2022), 2994–3013. https://doi.org/10.1002/mma.7973.

[32] M.-L. Kienle Garrido, T. Breitenbach, K. Chudej, A. Borzì, Modeling and Numerical Solution of a Cancer Therapy Optimal Control Problem, Appl. Math. 09 (2018), 985–1004. https://doi.org/10.4236/am.2018.98067.

[33] I. Podlubny, Fractional Differential Equations, Academic Press, San Diego, (1999).

[34] I. Podlubny, L. Dorcak, I. Kostial, On Fractional Derivatives, Fractional-Order Dynamic Systems and $PI^{\lambda}D^{\mu}$-Controllers, in: Proceedings of the 36th IEEE Conference on Decision and Control, IEEE, San Diego, 1997: pp. 4985–4990. https://doi.org/10.1109/CDC.1997.649841.

[35] J.M. Kimeu, Fractional Calculus: Definitions and Applications, Thesis, Western Kentucky University, (2009).

[36] A.A. Kilbas, Theory and Applications of Fractional Differential Equations, Elsevier, (2006).

[37] S.-M. Jung, Hyers-Ulam-Rassias Stability of Functional Equations in Nonlinear Analysis, Springer, New York, 2011. https://doi.org/10.1007/978-1-4419-9637-4.

[38] M. Almuzini, I.M. Batiha, S. Momani, A Study of Fractional-Order Monkeypox Mathematical Model with Its Stability Analysis, in: 2023 International Conference on Fractional Differentiation and Its Applications (ICFDA), IEEE, Ajman, United Arab Emirates, 2023: pp. 1–6. https://doi.org/10.1109/ICFDA58234.2023.10153214.

[39] I.M. Batiha, A. Bataihah, A.A. Al-Nana, et al. A Numerical Scheme for Dealing With Fractional Initial Value Problem, Int. J. Innov. Comput. Inf. Control 19 (2023), 763–774.

[40] A. Zraiqat, S.K. Paikray, H. Dutta, A Certain Class of Deferred Weighted Statistical B-Summability Involving (p,q)-Integers and Analogous Approximation Theorems, Filomat 33 (2019), 1425–1444. https://doi.org/10.2298/FIL1905425Z.

[41] Statistics Times, Countries by GDP Growth, 2020. https://statisticstimes.com (accessed on 15 March 2023).

[42] P. van den Driessche, Reproduction Numbers of Infectious Disease Models, Infect. Dis. Model. 2 (2017), 288–303. https://doi.org/10.1016/j.idm.2017.06.002.